Spontaneous corrugation of dipolar membranes

Xiuquan Sun and J. Daniel Gezelter*
Department of Chemistry and Biochemistry, University of Notre Dame, Notre Dame, Indiana 46556, USA
(Received 13 October 2006; revised manuscript received 29 December 2006; published 26 March 2007)

We present a simple model for dipolar elastic membranes that gives lattice-bound point dipoles complete orientational freedom as well as translational freedom along one coordinate (out of the plane of the membrane). There is an additional harmonic term which binds each of the dipoles to the six nearest neighbors on either triangular or distorted lattices. The translational freedom of the dipoles allows triangular lattices to find states that break out of the normal orientational disorder of frustrated configurations and which are stabilized by long-range antiferroelectric ordering. In order to break out of the frustrated states, the dipolar membranes form corrugated or "rippled" phases that make the lattices effectively nontriangular. We observe three common features of the corrugated dipolar membranes: (1) the corrugated phases develop easily when hosted on triangular lattices, (2) the wave vectors for the surface ripples are always found to be perpendicular to the dipole director axis, and (3) on triangular lattices, the dipole director axis is found to be parallel to any of the three equivalent lattice directions.

DOI: 10.1103/PhysRevE.75.031602 PACS number(s): 68.03.Hj, 82.20.Wt

I. INTRODUCTION

The properties of polymeric membranes are known to depend sensitively on the details of the internal interactions between the constituent monomers. A flexible membrane will always have a competition between the energy of curvature and the in-plane stretching energy and will be able to buckle in certain limits of surface tension and temperature [1]. The buckling can be nonspecific and centered at dislocation [2] or grain-boundary defects [3], or it can be directional and cause long "roof-tile" or tubelike structures to appear in partially polymerized phospholipid vesicles [4].

One would expect that anisotropic local interactions could lead to interesting properties of the buckled membrane. We report here on the buckling behavior of a membrane composed of harmonically bound, but freely rotating electrostatic dipoles. The dipoles have strongly anisotropic local interactions and the membrane exhibits coupling between the buckling and the long-range ordering of the dipoles.

Buckling behavior in liquid crystalline and biological membranes is a well-known phenomenon. Relatively pure phosphatidylcholine (PC) bilayers form a corrugated or "rippled" phase ($P_{\beta'}$) which appears as an intermediate phase between the gel (L_β) and fluid (L_α) phases. The $P_{\beta'}$ phase has attracted substantial experimental interest over the past 30 years. Most structural information of the ripple phase has been obtained by the x-ray diffraction [5,6] and freeze-fracture electron microscopy (FFEM) [7,8]. Recently, Kaasgaard *et al.* used atomic force microscopy (AFM) to observe ripple phase morphology in bilayers supported on mica [9]. The experimental results provide strong support for a two-dimensional (2D) triangular packing lattice of the lipid molecules within the ripple phase. This is a notable change from the observed lipid packing within the gel phase [10]. There have been a number of theoretical approaches [11–18] (and some heroic simulations [19–23]) undertaken to try to explain this phase, but to date, none have looked specifically at the contribution of the dipolar character of the lipid head groups towards this corrugation. Lipid chain interdigitation certainly plays a major role, and the structures of the ripple phase are highly ordered. The model we investigate here lacks chain interdigitation (as well as the chains themselves) and will not be detailed enough to rule in favor of (or against) any of these explanations for the $P_{\beta'}$ phase.

Membranes containing electrostatic dipoles can also exhibit the flexoelectric effect [24–26], which is the ability of mechanical deformations to result in electrostatic organization of the membrane. This phenomenon is a curvature-induced membrane polarization which can lead to potential differences across a membrane. Reverse flexoelectric behavior (in which applied currents effect membrane curvature) has also been observed. Explanations of the details of these effects have typically utilized membrane polarization perpendicular to the face of the membrane [26], and the effect has been observed in both biological [27], bent-core liquid crystalline [25], and polymer-dispersed liquid crystalline membranes [24].

The problem with using atomistic and even coarse-grained approaches to study membrane buckling phenomena is that only a relatively small number of periods of the corrugation (i.e., one or two) can be realistically simulated given current technology. Also, simulations of lipid bilayers are traditionally carried out with periodic boundary conditions in two or three dimensions and these have the potential to enhance the periodicity of the system at that wavelength. To avoid this pitfall, we are using a model which allows us to have sufficiently large systems so that we are not causing artificial corrugation through the use of periodic boundary conditions.

The simplest dipolar membrane is one in which the dipoles are located on fixed lattice sites. Ferroelectric states (with long-range dipolar order) can be observed in dipolar systems with nontriangular packings. However, *triangularly* packed 2D dipolar systems are inherently frustrated and one would expect a dipolar-disordered phase to be the lowest free

*Electronic address: gezelter@nd.edu

energy configuration [28,29]. Dipolar lattices already have rich phase behavior, but in order to allow the membrane to buckle, a single degree of freedom (translation normal to the membrane face) must be added to each of the dipoles. It would also be possible to allow complete translational freedom. This approach is similar in character to a number of elastic Ising models that have been developed to explain interesting mechanical properties in magnetic alloys [30–33].

What we present here is an attempt to find the simplest dipolar model which will exhibit buckling behavior. We are using a modified *XYZ* lattice model; details of the model can be found in Sec. II, results of Monte Carlo simulations using this model are presented in Sec. III, and Sec. IV contains our conclusions.

II. TWO-DIMENSIONAL DIPOLAR MEMBRANE

The point of developing this model was to arrive at the simplest possible theoretical model which could exhibit spontaneous corrugation of a two-dimensional dipolar medium. Since molecules in polymerized membranes and in the $P_{\beta'}$ ripple phase have limited translational freedom, we have chosen a lattice to support the dipoles in the x-y plane. The lattice may be either triangular (lattice constants $a/b=\sqrt{3}$) or distorted. However, each dipole has 3 degrees of freedom. They may move freely *out* of the x-y plane (along the z axis), and they have complete orientational freedom ($0<=\theta<=\pi$, $0<=\phi<2\pi$). This is essentially a modified *X-Y-Z* model with translational freedom along the z axis.

The potential energy of the system,

$$V=\sum_i\left(\sum_{j>i}\frac{|\mu|^2}{4\pi\epsilon_0 r_{ij}^3}[\hat{\mathbf{u}}_i\cdot\hat{\mathbf{u}}_j-3(\hat{\mathbf{u}}_i\cdot\hat{\mathbf{r}}_{ij})(\hat{\mathbf{u}}_j\cdot\hat{\mathbf{r}}_{ij})]+\sum_{j\in NN_i}^{6}\frac{k_r}{2}(r_{ij}-\sigma)^2\right). \tag{2.1}$$

In this potential, $\hat{\mathbf{u}}_i$ is the unit vector pointing along dipole i and $\hat{\mathbf{r}}_{ij}$ is the unit vector pointing along the interdipole vector $\mathbf{r}_{ij}$. The entire potential is governed by three parameters, the dipolar strength (μ), the harmonic spring constant (k_r), and the preferred intermolecular spacing (σ). In practice, we set the value of σ to the average intermolecular spacing from the planar lattice, yielding a potential model that has only two parameters for a particular choice of lattice constants a (along the x axis) and b (along the y axis). We also define a set of reduced parameters based on the length scale (σ) and the energy of the harmonic potential at a deformation of 2σ ($\epsilon=k_r\sigma^2/2$). Using these two constants, we perform our calculations using reduced distances ($r^*=r/\sigma$), temperatures ($T^*=2k_BT/k_r\sigma^2$), densities ($\rho^*=N\sigma^2/L_xL_y$), and dipole moments ($\mu^*=\mu/\sqrt{4\pi\epsilon_0\sigma^5k_r/2}$). It should be noted that the density (ρ^*) depends only on the mean particle spacing in the x-y plane; the lattice is fully populated.

To investigate the phase behavior of this model, we have performed a series of Metropolis Monte Carlo simulations of moderately sized (34.3σ on a side) patches of membrane hosted on both triangular ($\gamma=a/b=\sqrt{3}$) and distorted ($\gamma\neq\sqrt{3}$) lattices. The linear extent of one edge of the monolayer was $20a$ and the system was kept roughly square. The average distance that coplanar dipoles were positioned from their six nearest neighbors was 1σ (on both triangular and distorted lattices). Typical system sizes were 1360 dipoles for the triangular lattices and 840–2800 dipoles for the distorted lattices. Two-dimensional periodic boundary conditions were used, and the cutoff for the dipole-dipole interaction was set to 4.3σ. This cutoff is roughly 2.5 times the typical real-space electrostatic cutoff for molecular systems. Since dipole-dipole interactions decay rapidly with distance, and since the intrinsic three-dimensional periodicity of the Ewald sum can give artifacts in 2D systems, we have chosen not to use it in these calculations. Although the Ewald sum has been reformulated to handle 2D systems [34–38], these methods are computationally expensive [39,40], and are not necessary in this case. All parameters (T^*, μ^*, and γ) were varied systematically to study the effects of these parameters on the formation of ripplelike phases.

III. RESULTS AND ANALYSIS

A. Dipolar ordering and coexistence temperatures

The principal method for observing the orientational ordering transition in dipolar systems is the P_2 order parameter (defined as $1.5\times\lambda_{\max}$), where $\lambda_{\max}$ is the largest eigenvalue of the matrix,

$$\mathsf{S}=\frac{1}{N}\sum_i\begin{pmatrix}u_i^xu_i^x-\frac{1}{3} & u_i^xu_i^y & u_i^xu_i^z\\ u_i^yu_i^x & u_i^yu_i^y-\frac{1}{3} & u_i^yu_i^z\\ u_i^zu_i^x & u_i^zu_i^y & u_i^zu_i^z-\frac{1}{3}\end{pmatrix}. \tag{3.1}$$

Here u_i^α is the $\alpha=x,y,z$ component of the unit vector for dipole i. P_2 will be 1.0 for a perfectly ordered system and near 0 for a randomized system. Note that this order parameter is *not* equal to the polarization of the system. For example, the polarization of the perfect antiferroelectric system is 0, but P_2 for an antiferroelectric system is 1. The eigenvector of S corresponding to the largest eigenvalue is familiar as the director axis, which can be used to determine a privileged dipolar axis for dipole-ordered systems. The top panel in Fig. 1 shows the values of P_2 as a function of temperature for both triangular ($\gamma=1.732$) and distorted ($\gamma=1.875$) lattices.

There is a clear order-disorder transition in evidence from this data. Both the triangular and distorted lattices have dipolar-ordered low-temperature phases, and orientationally disordered high-temperature phases. The coexistence temperature for the triangular lattice is significantly lower than for the distorted lattices, and the bulk polarization is approximately 0 for both dipolar ordered and disordered phases. This gives strong evidence that the dipolar ordered phase is antiferroelectric. We have verified that this dipolar ordering transition is not a function of system size by performing identical calculations with systems 2 times as large. The transition is equally smooth at all system sizes that were studied. Additionally, we have repeated the Monte Carlo simulations over a wide range of lattice ratios (γ) to generate a dipolar

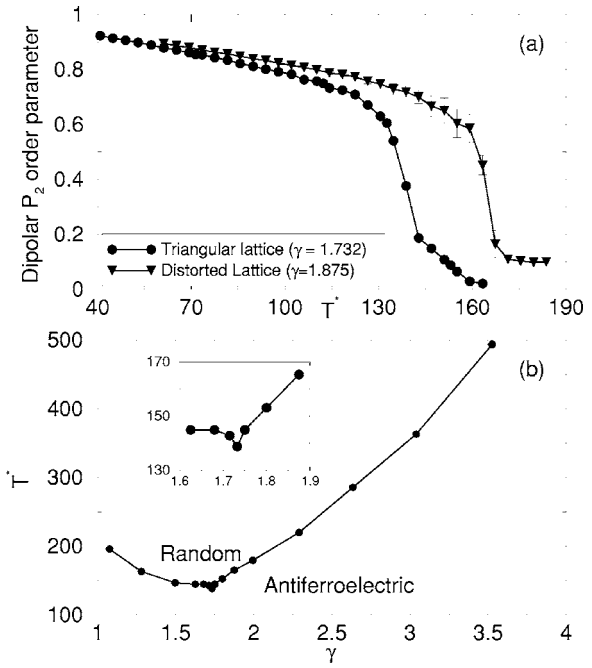

FIG. 1. Top panel: The P_2 dipolar order parameter as a function of temperature for both triangular (γ=1.732) and distorted (γ =1.875) lattices. Bottom panel: The phase diagram for the dipolar membrane model. The line denotes the division between the dipolar ordered (antiferroelectric) and disordered phases. An enlarged view near the triangular lattice is shown by the inset.

order-disorder phase diagram. The bottom panel in Fig. 1 shows that the triangular lattice is a low-temperature cusp in the T^*-γ phase diagram.

This phase diagram is remarkable in that it shows an antiferroelectric phase near γ=1.732 where one would expect lattice frustration to result in disordered phases at all temperatures. Observations of the configurations in this phase show clearly that the system has accomplished dipolar ordering by forming large ripplelike structures. We have observed antiferroelectric ordering in all three of the equivalent directions on the triangular lattice, and the dipoles have been observed to organize perpendicular to the membrane normal (in the plane of the membrane). It is particularly interesting to note that the ripplelike structures have also been observed to propagate in the three equivalent directions on the lattice, but the *direction of ripple propagation is always perpendicular to the dipole director axis*. A snapshot of a typical antiferroelectric rippled structure is shown in Fig. 2.

Although the snapshot in Fig. 2 gives the appearance of three-row stairlike structures, these appear to be transient. On average, the corrugation of the membrane is a relatively smooth, long-wavelength phenomenon, with occasional steep drops between adjacent lines of antialigned dipoles.

The height-dipole correlation function $[C_{\mathrm{hd}}(r,\cos\theta)]$ makes the connection between dipolar ordering and the wave vector of the ripple even more explicit. $C_{\mathrm{hd}}(r,\cos\theta)$ is an angle-dependent pair distribution function. The angle (θ) is the angle between the intermolecular vector $\vec{r}_{ij}$ and direction of dipole i,

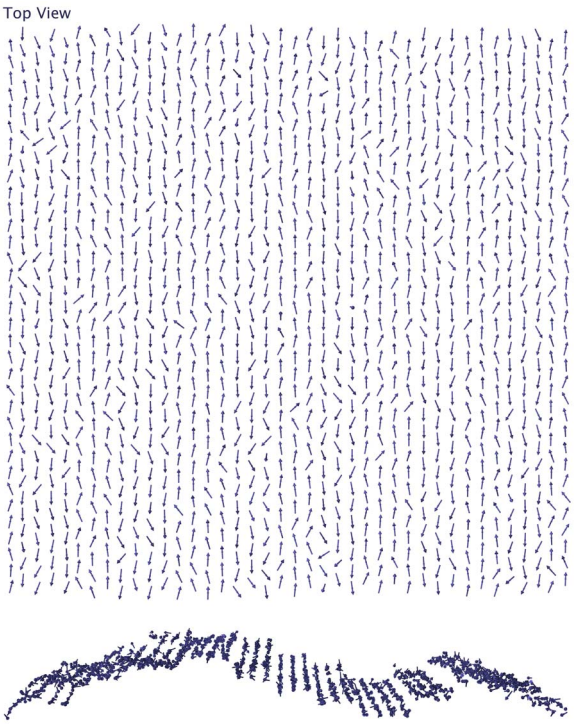

FIG. 2. (Color online) Top and side views of a representative configuration for the dipolar ordered phase supported on the triangular lattice. Note the antiferroelectric ordering and the long wavelength buckling of the membrane. Dipolar ordering has been observed in all three equivalent directions on the triangular lattice, and the ripple direction is always perpendicular to the director axis for the dipoles.

$$C_{\mathrm{hd}} = \frac{\left\langle \frac{1}{n(r)} \sum_i \sum_{j>i} h_i \cdot h_j \delta(r - r_{ij}) \delta(\cos\theta_{ij} - \cos\theta) \right\rangle}{\langle h^2 \rangle}, \tag{3.2}$$

where $\cos\theta_{ij} = \hat{\mu}_i \cdot \hat{r}_{ij}$ and $\hat{r}_{ij} = \vec{r}_{ij}/r_{ij}$. $n(r)$ is the number of dipoles found in a cylindrical shell between r and $r+\delta r$ of the central particle. Figure 3 shows contours of this correlation function for both antiferroelectric, rippled membranes as well as for the dipole-disordered portion of the phase diagram.

The height-dipole corrselation function gives a map of how the topology of the membrane surface varies with angular deviation around a given dipole. The upper panel of Fig. 3 shows that in the antiferroelectric phase, the dipole heights are strongly correlated for dipoles in head-to-tail arrangements, and this correlation persists for very long distances (up to 15 σ). For portions of the membrane located perpendicular to a given dipole, the membrane height becomes anticorrelated at distances of 10σ. The correlation function is relatively smooth; there are no steep jumps or steps, so the stairlike structures in Fig. 2 are indeed transient and disappear when averaged over many configurations. In the dipole-disordered phase, the height-dipole correlation function is relatively flat (and hovers near zero). The only

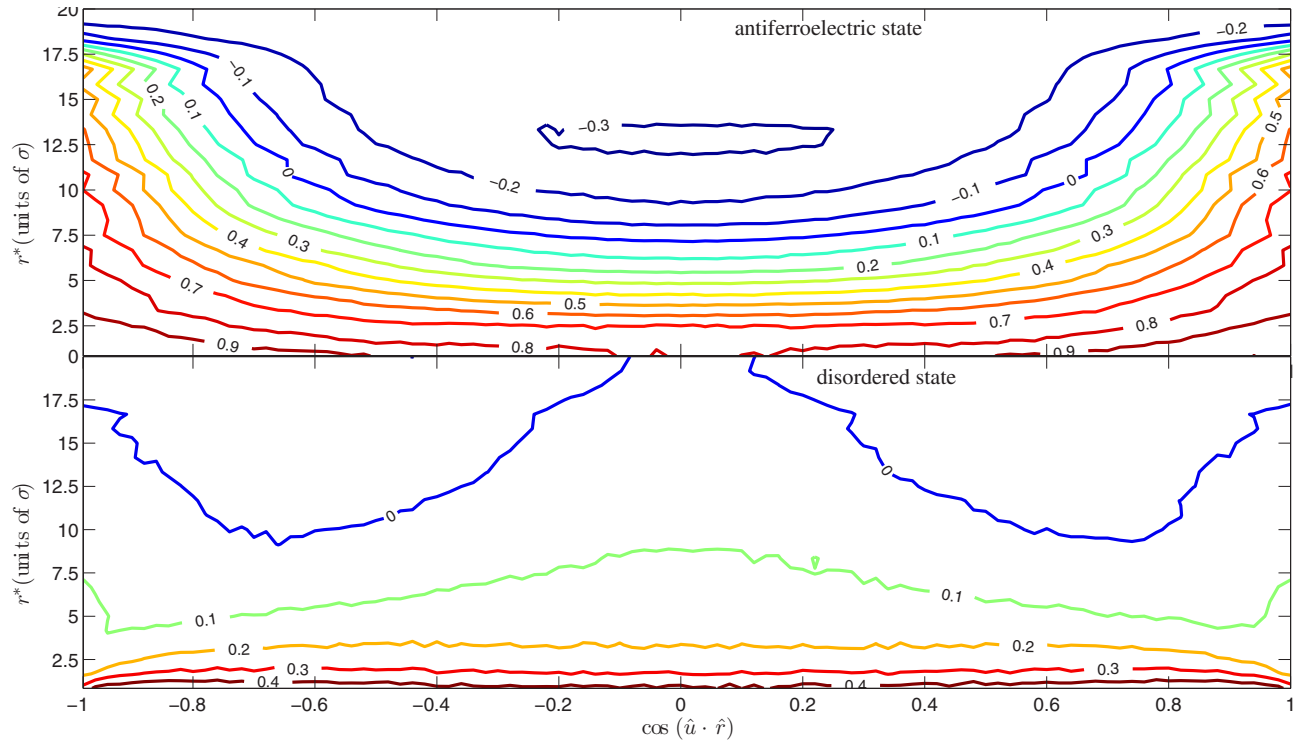

FIG. 3. (Color online) Contours of the height-dipole correlation function as a function of the dot product between the dipole ($\hat{\mu}$) and interdipole separation vector ($\hat{r}$) and the distance (r) between the dipoles. Perfect height correlation (contours approaching 1) are present in the ordered phase when the two dipoles are in the same head-to-tail line. Anticorrelation (contours below 0) is only seen when the interdipole vector is perpendicular to the dipoles. In the dipole-disordered portion of the phase diagram, there is only weak correlation in the dipole direction and this correlation decays rapidly to zero for intermolecular vectors that are not dipole aligned.

significant height correlations are for axial dipoles at very short distances ($r \approx \sigma$).

B. Discriminating ripples from thermal undulations

In order to be sure that the structures we have observed are actually a rippled phase and not simply thermal undulations, we have computed the undulation spectrum,

$$h(\vec{q}) = A^{-1/2} \int d\vec{r} h(\vec{r}) e^{-i\vec{q}\cdot\vec{r}}, \tag{3.3}$$

where $h(\vec{r})$ is the height of the membrane at location $\vec{r} = (x,y)$ [1,41]. In simple (and more complicated) elastic continuum models, it can shown that in the *NVT* ensemble, the absolute value of the undulation spectrum can be written as

$$\langle |h(q)|^2 \rangle_{NVT} = \frac{k_B T}{k_c q^4 + \gamma q^2}, \tag{3.4}$$

where k_c is the bending modulus for the membrane, and γ is the mechanical surface tension [1]. The systems studied in this paper have essentially zero bending moduli (k_c) and relatively large mechanical surface tensions (γ), so a much simpler form can be written as

$$\langle |h(q)|^2 \rangle_{NVT} = \frac{k_B T}{\gamma q^2}, \tag{3.5}$$

The undulation spectrum is computed by superimposing a rectangular grid on top of the membrane, and by assigning height [$h(\vec{r})$] values to the grid from the average of all dipoles that fall within a given $\vec{r}+d\vec{r}$ grid area. Empty grid pixels are assigned height values by interpolation from the nearest-neighbor pixels. A standard 2D Fourier transform is then used to obtain $\langle |h(q)|^2 \rangle$. Alternatively, since the dipoles sit on a Bravais lattice, one could use the heights of the lattice points themselves as the grid for the Fourier transform (without interpolating to a square grid). However, if lateral translational freedom is added to this model (a likely extension), an interpolated grid method for computing undulation spectra will be required.

As mentioned above, the best fits to our undulation spectra are obtained by setting the value of k_c to 0. In Fig. 4 we show typical undulation spectra for two different regions of the phase diagram along with their fits from the Landau free energy approach [Eq. (3.5)]. In the high-temperature disordered phase, the Landau fits can be nearly perfect, and from these fits we can estimate the tension in the surface. In reduced units, typical values of $\gamma^* = \gamma/\epsilon = 2500$ are obtained for the disordered phase ($\gamma^* = 2551.7$ in the top panel of Fig. 4).

Typical values of γ^* in the dipolar-ordered phase are much higher than in the dipolar-disordered phase ($\gamma^* = 73\,538$ in the lower panel of Fig. 4). For the dipolar-ordered triangular lattice near the coexistence temperature, we also observe long wavelength undulations that are far outliers to the fits. That is, the Landau free energy fits are well within error bars for most of the other points, but can be off by *orders of magnitude* for a few low frequency components.

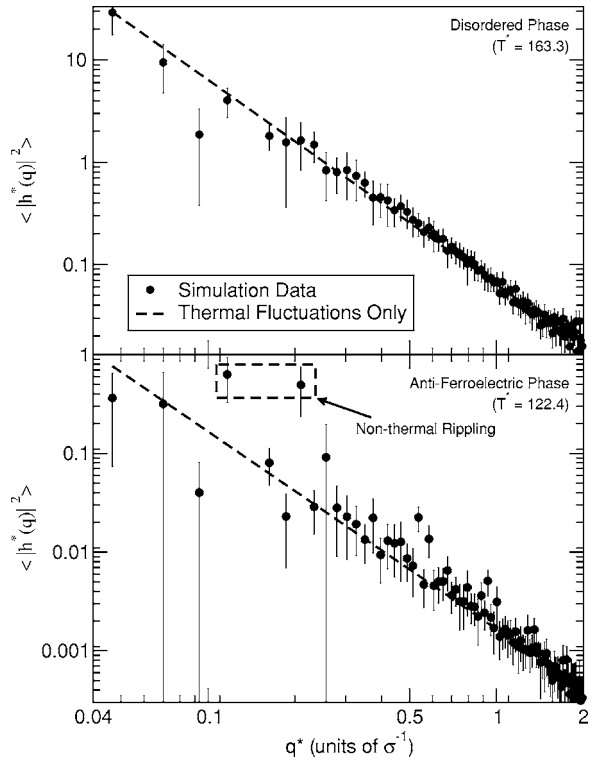

FIG. 4. Evidence that the observed ripples are *not* thermal undulations is obtained from the 2D Fourier transform $\langle|h^*(\vec{q})|^2\rangle$ of the height profile $[\langle h^*(x,y)\rangle]$. Rippled samples show low-wavelength peaks that are outliers on the Landau free energy fits by an order of magnitude. Samples exhibiting only thermal undulations fit Eq. (3.4) remarkably well.

We interpret these outliers as evidence that these low frequency modes are *non thermal undulations*. We take this as evidence that we are actually seeing a rippled phase developing in this model system.

C. Effects of potential parameters on amplitude and wavelength

We have used two different methods to estimate the amplitude and periodicity of the ripples. The first method requires projection of the ripples onto a one-dimensional rippling axis. Since the rippling is always perpendicular to the dipole director axis, we can define a ripple vector as follows. The largest eigenvector, s_1, of the S matrix in Eq. (3.1) is projected onto a planar director axis,

$$\vec{d} = \begin{pmatrix} \vec{s}_1 \cdot \hat{i} \\ \vec{s}_1 \cdot \hat{j} \\ 0 \end{pmatrix} \tag{3.6}$$

($\hat{i}$, $\hat{j}$, and $\hat{k}$ are unit vectors along the x, y, and z axes, respectively). The rippling axis is in the plane of the membrane and is perpendicular to the planar director axis,

$$\vec{q}_{\text{rip}} = \vec{d} \times \hat{k}. \tag{3.7}$$

We can then find the height profile of the membrane along the ripple axis by projecting heights of the dipoles to obtain a one-dimensional height profile, $h(q_{\text{rip}})$. Ripple wavelengths can be estimated from the largest nonthermal low-frequency component in the Fourier transform of $h(q_{\text{rip}})$. Amplitudes can be estimated by measuring peak-to-trough distances in $h(q_{\text{rip}})$ itself.

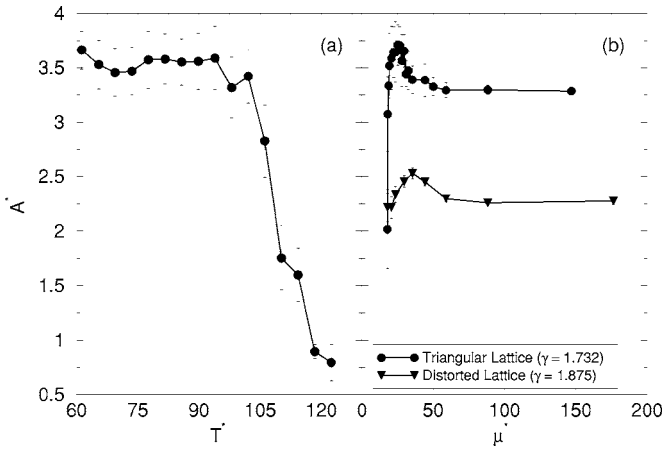

FIG. 5. (a) The amplitude A^* of the ripples vs temperature for a triangular lattice. (b) The amplitude A^* of the ripples vs dipole strength (μ^*) for both the triangular lattice (circles) and distorted lattice (squares). The reduced temperatures were kept fixed at $T^*=94$ for the triangular lattice and $T^*=106$ for the distorted lattice (approximately 2/3 of the order-disorder transition temperature for each lattice).

A second, more accurate, and simpler method for estimating ripple shape is to extract the wavelength and height information directly from the largest nonthermal peak in the undulation spectrum. For large-amplitude ripples, the two methods give similar results. The one-dimensional projection method is more prone to noise (particularly in the amplitude estimates for the distorted lattices). We report amplitudes and wavelengths taken directly from the undulation spectrum below.

In the triangular lattice ($\gamma=\sqrt{3}$), the rippling is observed for temperatures (T^*) from 61–122. The wavelength of the ripples is remarkably stable at 21.4σ for all but the temperatures closest to the order-disorder transition. At $T^*=122$, the wavelength drops to 17.1σ.

The dependence of the amplitude on temperature is shown in the top panel of Fig. 5. The rippled structures shrink smoothly as the temperature rises towards the order-disorder transition. The wavelengths and amplitudes we observe are surprisingly close to the $\Lambda/2$ phase observed by Kaasgaard *et al.* in their work on PC-based lipids [9]. However, this is coincidental agreement based on a choice of 7 Å as the mean spacing between lipids.

The ripples can be made to disappear by increasing the internal elastic tension (i.e., by increasing k_r or equivalently, reducing the dipole moment). The amplitude of the ripples depends critically on the strength of the dipole moments (μ^*) in Eq. (2.1). If the dipoles are weakened substantially (below $\mu^*=20$) at a fixed temperature of 94, the membrane loses dipolar ordering and the ripple structures. The ripples reach a peak amplitude of 3.7σ at a dipolar strength of 25. We show the dependence of ripple amplitude on the dipolar strength in Fig. 5.

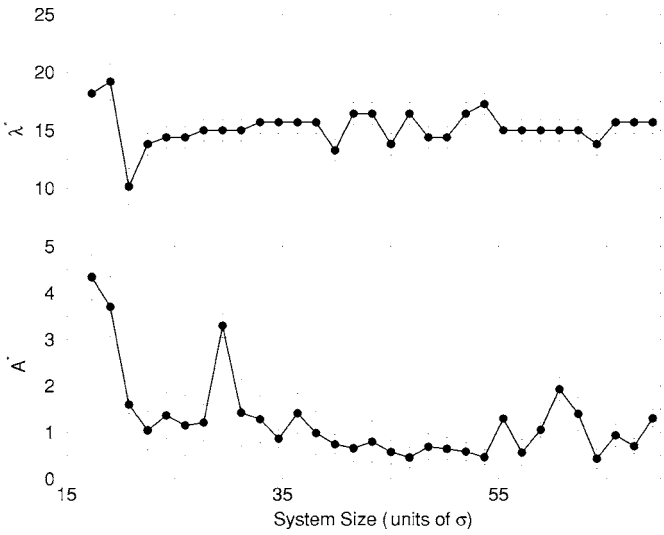

FIG. 6. The ripple wavelength (top) and amplitude (bottom) as a function of system size for a triangular lattice (γ=1.732) at T^* =122.

D. Distorted lattices

We have also investigated the effect of the lattice geometry by changing the ratio of lattice constants (γ) while keeping the average nearest-neighbor spacing constant. The antiferroelectric state is accessible for all γ values we have used, although the distorted triangular lattices prefer a particular director axis due to the anisotropy of the lattice.

Our observation of rippling behavior was not limited to the triangular lattices. In distorted lattices the antiferroelectric phase can develop nearly instantaneously in the Monte Carlo simulations, and these dipolar-ordered phases tend to be remarkably flat. Whenever rippling has been observed in these distorted lattices (e.g., γ=1.875), we see relatively short ripple wavelengths (14σ) and amplitudes of 2.4σ. These ripples are weakly dependent on dipolar strength (see Fig. 5), although below a dipolar strength of $\mu^*=20$, the membrane loses dipolar ordering and displays only thermal undulations.

The ripple phase does *not* appear at all values of γ. We have only observed nonthermal undulations in the range $1.625<\gamma<1.875$. Outside this range, the order-disorder transition in the dipoles remains, but the ordered dipolar phase has only thermal undulations. This is one of our strongest pieces of evidence that rippling is a symmetry-breaking phenomenon for triangular and nearly triangular lattices.

E. Effects of system size

To evaluate the effect of finite system size, we have performed a series of simulations on the triangular lattice at a reduced temperature of 122, which is just below the order-disorder transition temperature ($T^*=139$). These conditions are in the dipole-ordered and rippled portion of the phase diagram. These are also the conditions that should be most susceptible to system size effects.

There is substantial dependence on system size for small (less than 29σ) periodic boxes. Notably, there are resonances apparent in the ripple amplitudes at box lengths of 17.3σ and 29.5σ. For larger systems, the behavior of the ripples appears to have stabilized and is on a trend to slightly smaller amplitudes (and slightly longer wavelengths) than were observed from the 34.3σ box sizes that were used for most of the calculations. Fig 6 summarizes the effects of system size on ripple wavelength and amplitude.

It is interesting to note that system sizes which are multiples of the default ripple wavelength can enhance the amplitude of the observed ripples, but appears to have only a minor effect on the observed wavelength. It would, of course, be better to use system sizes that were many multiples of the ripple wavelength to be sure that the periodic box is not driving the phenomenon, but at the largest system size studied ($70\sigma\times70\sigma$), the number of dipoles (5440) made long Monte Carlo simulations prohibitively expensive.

IV. DISCUSSION

We have been able to show that a simple dipolar lattice model which contains only molecular packing (from the lattice), anisotropy (in the form of electrostatic dipoles) and a weak elastic tension (in the form of a nearest-neighbor harmonic potential), is capable of exhibiting stable long-wavelength nonthermal surface corrugations. The best explanation for this behavior is that the ability of the dipoles to translate out of the plane of the membrane is enough to break the symmetry of the triangular lattice and allow the energetic benefit from the formation of a bulk antiferroelectric phase. Were the weak elastic tension absent from our model, it would be possible for the entire lattice to "tilt" using z translation. Tilting the lattice in this way would yield an effectively nontriangular lattice which would avoid dipolar frustration altogether. With the elastic tension in place, bulk tilt causes a large strain, and the least costly way to release this strain is between two rows of antialigned dipoles. These "breaks" will result in rippled or sawtooth patterns in the membrane, and allow small stripes of membrane to form antiferroelectric regions that are tilted relative to the averaged membrane normal.

Although the dipole-dipole interaction is the major driving force for the long range orientational ordered state, the formation of the stable, smooth ripples is a result of the competition between the elastic tension and the dipole-dipole interactions. This statement is supported by the variation in μ^*. Substantially weaker dipoles relative to the surface tension can cause the corrugated phase to disappear.

The packing of the dipoles into a nearly triangular lattice is clearly an important piece of the puzzle. The dipolar head groups of lipid molecules are sterically (as well as electrostatically) anisotropic, and would not pack in triangular arrangements without the steric interference of adjacent molecular bodies. Since we only see rippled phases in the neighborhood of $\gamma=\sqrt{3}$, this implies that even if this dipolar mechanism is the correct explanation for the ripple phase in realistic bilayers, there would still be a role played by the lipid chains in the in-plane organization of the triangularly ordered phases which could support ripples. The present model is certainly not detailed enough to answer exactly

what drives the formation of the $P_{\beta'}$ phase in real lipids, but suggests some avenues for further experiments.

The most important prediction we can make using the results from this simple model is that if dipolar ordering is driving the surface corrugation, the wave vectors for the ripples should always be found to be *perpendicular* to the dipole director axis. This prediction should suggest experimental designs which test whether this is really true in the phosphatidylcholine $P_{\beta'}$ phases. The dipole director axis should also be easily computable for the all-atom and coarse-grained simulations that have been presented in the literature.

Our other observation about the ripple and dipolar directionality is that the dipole director axis can be found to be parallel to any of the three equivalent lattice vectors in the triangular lattice. Defects in the ordering of the dipoles can cause the dipole director (and consequently the surface corrugation) of small regions to be rotated relative to each other by 120°. This is a similar behavior to the domain rotation seen in the AFM studies of Kaasgaard *et al.* [9].

Although our model is simple, it exhibits some rich and unexpected behaviors. It would clearly be a closer approximation to the reality if we allowed greater translational freedom to the dipoles and replaced the somewhat artificial lattice packing and the harmonic elastic tension with more realistic molecular modeling potentials. What we have done is to present a simple model which exhibits bulk nonthermal corrugation, and our explanation of this rippling phenomenon will help us design more accurate molecular models for corrugated membranes and experiments to test whether rippling is dipole driven or not.

ACKNOWLEDGMENTS

Support for this project was provided by the National Science Foundation under Grant No. CHE-0134881. The authors would like to thank the reviewers for helpful comments.

[1] S. A. Safran, *Statistical Thermodynamics of Surfaces, Interfaces, and Membranes* (Addison-Wesley, Reading, MA, 1994).
[2] H. S. Seung and D. R. Nelson, Phys. Rev. A **38**, 1005 (1988).
[3] C. Carraro and D. R. Nelson, Phys. Rev. E **48**, 3082 (1993).
[4] M. Mutz, D. Bensimon, and M. J. Brienne, Phys. Rev. Lett. **67**, 923 (1991).
[5] W. J. Sun, S. Tristram-Nagle, R. M. Suter, and J. F. Nagle, Proc. Natl. Acad. Sci. U.S.A. **93**, 7008 (1996).
[6] J. Katsaras, S. Tristram-Nagle, Y. Liu, R. L. Headrick, E. Fontes, P. C. Mason, and J. F. Nagle, Phys. Rev. E **61**, 5668 (2000).
[7] B. R. Copeland and H. M. McConnell, Biochim. Biophys. Acta **599**, 95 (1980).
[8] H. W. Meyer, Biochim. Biophys. Acta **1302**, 221 (1996).
[9] T. Kaasgaard, C. Leidy, J. H. Crowe, O. G. Mouritsen, and K. Jorgensen, Biophys. J. **85**, 350 (2003).
[10] G. Cevc and D. Marsh, *Phospholipid Bilayers* (Wiley-Interscience, New York, 1980).
[11] M. Marder, H. L. Frisch, J. S. Langer, and H. M. McConnell, Proc. Natl. Acad. Sci. U.S.A. **81**, 6559 (1984).
[12] R. E. Goldstein and S. Leibler, Phys. Rev. Lett. **61**, 2213 (1988).
[13] W. S. McCullough and H. L. Scott, Phys. Rev. Lett. **65**, 931 (1990).
[14] T. C. Lubensky and F. C. MacKintosh, Phys. Rev. Lett. **71**, 1565 (1993).
[15] C. Misbah, J. Duplat, and B. Houchmandzadeh, Phys. Rev. Lett. **80**, 4598 (1998).
[16] T. Heimburg, Biophys. J. **78**, 1154 (2000).
[17] K. Kubica, Comput. Chem. (Oxford) **26**, 351 (2002).
[18] S. Bannerjee, Physica A **308**, 89 (2002).
[19] G. Ayton and G. A. Voth, Biophys. J. **83**, 3357 (2002).
[20] F. Y. Jiang, Y. Bouret, and J. T. Kindt, Biophys. J. **87**, 182 (2004).
[21] G. Brannigan and F. L. H. Brown, J. Chem. Phys. **120**, 1059 (2004).
[22] A. H. de Vries, S. Yefimov, A. E. Mark, and S. J. Marrink, Proc. Natl. Acad. Sci. U.S.A. **102**, 5392 (2005).
[23] J. de Joannis, F. Y. Jiang, and J. T. Kindt, Langmuir **22**, 998 (2006).
[24] L. Todorova, T. Angelov, Y. Marinov, and A. G. Petrov, J. Mater. Sci.: Mater. Electron. **14**, 817 (2004).
[25] J. Harden, B. Mbanga, N. Eber, K. Fodor-Csorba, S. Sprunt, J. T. Gleeson, and A. Jakli, Phys. Rev. Lett. **97**, 157802 (2006).
[26] A. G. Petrof, Anal. Chim. Acta **568**, 70 (2006).
[27] R. M. Raphael, A. S. Popel, and W. E. Brownell, Biophys. J. **78**, 2844 (2000).
[28] G. Toulouse, Commun. Phys. (London) **2**, 115 (1977).
[29] L. G. Marland and D. D. Betts, Phys. Rev. Lett. **43**, 1618 (1979).
[30] R. Renard and C. W. Garland, J. Chem. Phys. **44**, 1125 (1966).
[31] X. Zhu, F. Tavazza, and D. P. Landau, Phys. Rev. B **72**, 104102 (2005).
[32] X. Zhu and D. P. Landau, Phys. Rev. B **73**, 064115 (2006).
[33] Y. Jiang and T. Emig, Phys. Rev. B **73**, 104452 (2006).
[34] D. E. Parry, Surf. Sci. **49**, 433 (1975).
[35] D. E. Parry, Surf. Sci. **54**, 195 (1976).
[36] D. M. Heyes, M. Barber, and J. H. R. Clarke, J. Chem. Soc., Faraday Trans. 2 **73**, 1485 (1977).
[37] S. W. de Leeuw and J. W. Perram, Mol. Phys. **37**, 1313 (1979).
[38] Y.-J. Rhee, J. W. Halley, J. Hautman, and A. Rahman, Phys. Rev. B **40**, 36 (1989).
[39] E. Spohr, J. Chem. Phys. **107**, 6342 (1997).
[40] I.-C. Yeh and M. L. Berkowitz, J. Chem. Phys. **111**, 3155 (1999).
[41] U. Seifert, Adv. Phys. **46**, 13 (1997).